
Learning image registration without images

Malte Hoffmann
MGH, HMS

Benjamin Billot
UCL

Juan Eugenio Iglesias
MGH, HMS, UCL, and CSAIL, MIT

Bruce Fischl
MGH, HMS, and CSAIL, MIT

Adrian V. Dalca
MGH, HMS, and CSAIL, MIT

Abstract

We introduce a learning strategy for contrast-invariant image registration without requiring imaging data. While classical registration methods accurately estimate the spatial correspondence between images, they solve a costly optimization problem for every image pair. Learning-based techniques are fast at test time, but can only register images with image contrast and geometric content that are similar to those available during training. We focus on removing this image-data dependency of learning methods. Our approach leverages a generative model for diverse label maps and images that exposes networks to a wide range of variability during training, forcing them to learn features invariant to image type (contrast). This strategy results in powerful networks trained to generalize to a broad array of real input images. We present extensive experiments, with a focus on 3D neuroimaging, showing that this strategy enables robust registration of arbitrary image contrasts without the need to retrain for new modalities. We demonstrate registration accuracy that most often surpasses the state of the art both within and across modalities, using a single model. Critically, we show that input labels from which we synthesize images need not be of actual anatomy: training on randomly generated geometric shapes also results in competitive registration performance, albeit slightly less accurate, while alleviating the dependency on real data of any kind. Our code is available at <http://voxelmorph.csail.mit.edu>.

1 Introduction

Image registration estimates spatial correspondences between image pairs and is a fundamental component of many medical image analysis pipelines involving data acquired across time, subjects, and modalities. For example, neuroimaging segmentation packages [21, 23, 50] often perform deformable registration to a probabilistic atlas before neuroanatomical structures are labeled. This work focuses on frameworks that are agnostic to image modality, and excel both at uni-modal registration (e.g. between two T1-weighted MRI scans), as well as multi-modal registration (e.g. between MRI acquired with different contrasts). Both are important in neuroimaging, where different contrasts are commonly acquired, such as T1w for visualizing anatomy or T2w for detecting abnormal fluids [45]. These scans need to be aligned within subjects and to an external template, possibly of another modality [62]. Throughout this paper, we use the terms *modality* and *contrast* interchangeably, to designate a mode of acquisition such as MRI variants, which can yield images of very different appearance for the same anatomy.

Classical registration approaches estimate a deformation field between two images by optimizing an objective that balances image similarity with field regularity [3, 5, 43, 48, 56, 59, 67]. While these methods provide strong theoretical background and can yield good results, the expensive optimization needs to be repeated for each image pair, and the optimization objective and strategy typically need to be adapted to suit the types of images being registered. Instead, learning-based registration uses

datasets of images to learn a function that maps an image pair to a deformation field aligning the images [6, 18, 24, 42, 55, 61, 72, 76]. These methods achieve sub-second GPU runtimes, and can improve accuracy and robustness to local minima. Unfortunately, they are limited to the image contrast available during training, and therefore do not perform well on unobserved (new) image types. For example, a model trained on pairs of T1w and T2w MRI scans will not accurately register T1w and proton-density weighted (PDw) pairs. With a focus on neuroimaging, we remove this constraint of learning methods of registering only image types available during training, and design an approach that generalizes to any *unseen* image contrast at test time.

Contribution. In this work we present SynthMorph, a general learning framework for modality-agnostic registration that can handle a wide variety of *unseen* image contrasts at test time. SynthMorph enables registration of image pairs both within and across contrasts, *without* the need for any real imaging data during training. We first introduce a generative model for random label maps of variable geometric shapes. Second, conditioned on these maps, or optionally given other maps of interest, we build on recent methods to generate images of arbitrary contrasts, deformations, and artifacts [10]. Third, we replace the typical image-based objective with a contrast-agnostic loss that measures label overlap. The resulting network learns general features contained within the synthesized image data, invariant to the contrast of a specific modality.

We focus on neuroimaging and demonstrate state-of-the-art performance and runtimes compared to existing learning-based and classical baselines. The proposed framework outperforms existing methods across MRI contrasts, even though the network has never been exposed to *any* real imaging data. We also study various aspects of the proposed method, including feature invariance and the effects of hyperparameters, architecture size, and simulation aspects. The code is available as part of the VoxelMorph library at <http://voxelmorph.csail.mit.edu>.

2 Related work

Classical methods. Deformable registration has been widely studied [3, 5, 7, 59, 67]. Classical strategies undergo an iterative procedure that estimates an optimal deformation field for each image pair. This involves maximizing an image-similarity metric, which compares the warped moving and fixed images, and a regularization term that encourages desirable deformation properties such as preservation of topology [43, 48, 56, 59]. Cost function and optimization strategies are typically chosen to suit a particular task. Simple similarity metrics such as mean squared difference (MSD) or normalized cross-correlation (CC) [5] are widely used, and often provide excellent accuracy for image pairs of the same contrast [37].

For registration across modalities, metrics such as mutual information (MI) [68] and correlation ratio [54] are often employed, although the accuracy achieved with these cross-contrast measures is not on par with the within-contrast accuracy of CC and MSD [34]. For some tasks, e.g. registering intra-operative ultrasound to MRI, estimating even approximate correspondences can be challenging [64]. Although not often used in neuroimaging, metrics based on patch similarity [26, 28, 46, 69, 74] and normalized gradient fields [38, 39, 60] outperform simpler metrics, e.g. on abdominal computer-tomography (CT). Other methods convert images to a supervoxel representation, which is then spatially matched instead of the images [29, 36]. Although our work also employs geometric shapes, we do not generate supervoxels from input images, but synthesize arbitrary patterns (and images) from scratch during training to encourage learning contrast-invariant features for spatial correspondence.

Unfortunately, classical registration methods solve an independent optimization problem for each image pair, omitting advantages of learning across data. Neuroimaging scans typically have millions of voxels, leading to runtimes of several minutes to hours, depending on computational resources and packages used.

Learning approaches. Learning-based techniques mostly use convolutional neural networks (CNNs) to learn a function that directly outputs the deformation field given an image pair. After training, evaluating this function is efficient, enabling fast registration. Supervised models learn to reproduce simulated warps or deformation fields estimated by classical methods [20, 41, 55, 61, 75, 76]. In contrast, unsupervised models minimize a loss similar to classical cost functions [6, 16, 17, 40] such as normalized MI (NMI) [25] for cross-contrast registration. In another multi-modal registration paradigm, networks are used to synthesize one modality from the other, so that within-modality losses can be used in subsequent nonlinear registration [9, 14, 34, 52, 58, 63].

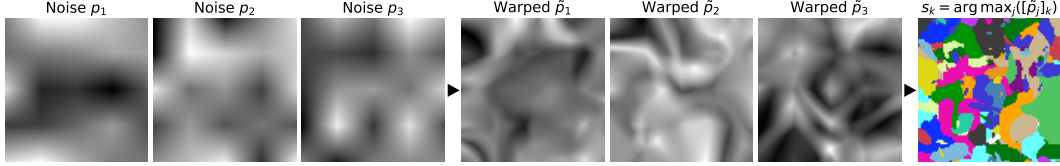


Figure 1: Generation of random input label maps. A set of smoothly varying 3D noise images p_j ($j \in \{1, 2, \dots, J\}$) is sampled from a standard distribution, then warped by random deformation fields ϕ_j to cover a range of spatial scales and shapes. A label map s is synthesized from the warped images $\tilde{p}_j = p_j \circ \phi_j$; for each voxel k of s , we determine in which \tilde{p}_j that voxel has the highest intensity, and assign the corresponding label j , i.e. $s_k = \arg \max_j ((\tilde{p}_j)_k)$. The example uses $J=26$.

Recent approaches also use segmentation-driven losses for registering different imaging modalities labeled during training, such as T2w MRI and 3D ultrasound, within the same subject [32, 33], or aiding existing formulations with auxiliary segmentation data [6, 30, 44].

Unfortunately, all these network-based approaches learn from image data seen during training and, consequently, do not perform well on unobserved modalities. Data augmentation strategies expose a model to a wider range of variability than the training data encompasses, for example by randomly altering voxel intensities or applying deformations [13, 57, 73, 78]. However, even these methods still need to sample data acquired with the target modality during training. Similarly, transfer learning can be used to extend a trained network to new modalities, but does not remove the need for some training data with the target contrast [35].

3 Method

3.1 Background

Let m and f be a moving and a fixed 3D image, respectively. We build on unsupervised learning-based registration frameworks and focus on deformable (non-linear) registration. These use a CNN h_θ with parameters θ that outputs the deformation $\phi_\theta = h_\theta(m, f)$ for image pair $\{m, f\}$.

In training, the network h_θ is given a pair of images $\{m, f\}$ at each iteration, and parameters are updated by optimizing a loss function $\mathcal{L}(\theta; m, f, \phi_\theta)$ similar to classical cost functions, using stochastic gradient descent. Typically, the loss contains an image dissimilarity term $\mathcal{L}_{dis}(m \circ \phi_\theta, f)$ which penalizes the difference between the warped image and the fixed in terms of appearance, and a regularization term $\mathcal{L}_{reg}(\phi)$ that encourages smooth deformations:

$$\mathcal{L}(\theta; m, f, \phi_\theta) = \mathcal{L}_{dis}(m \circ \phi_\theta, f) + \lambda \mathcal{L}_{reg}(\phi_\theta), \quad (1)$$

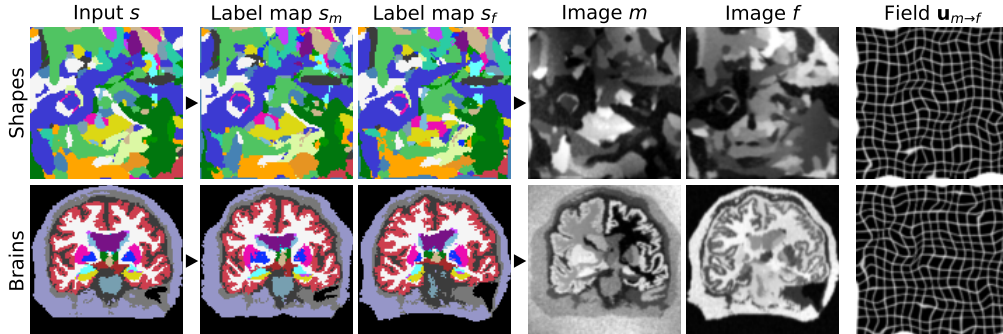


Figure 2: Data synthesis. Top: from random shapes. Bottom: if available, the synthesis can be initialized with anatomical labels. From an input label map s , we generate a pair of label maps $\{s_m, s_f\}$ and from them images $\{m, f\}$ with arbitrary contrast. The registration network takes $\{m, f\}$ as input to predict the displacement field $\mathbf{u}_{m \rightarrow f}$. In practice, if anatomical labels are available, we generate $\{s_m, s_f\}$ from two segmentations s from separate subjects.

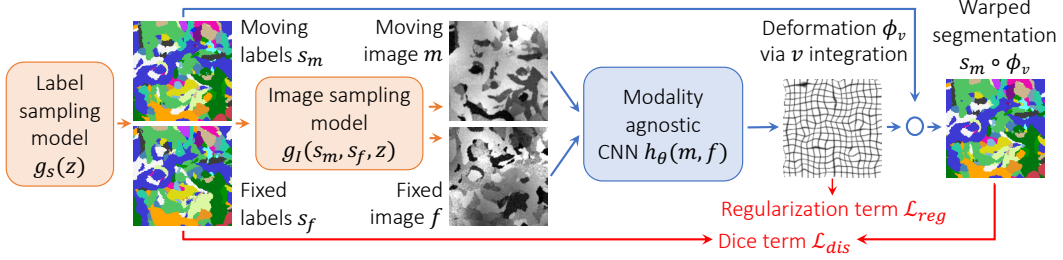


Figure 3: Proposed unsupervised learning framework for modality-agnostic diffeomorphic registration. We synthesize a pair of 3D label maps $\{s_m, s_f\}$ and then the corresponding 3D images $\{m, f\}$ based on a generative model that covers a wide range of shapes and contrasts. The images are used to train a U-Net-style network and the label maps are used in the loss to measure alignment.

where $\phi_\theta = h_\theta(m, f)$ is the network output, and λ controls the weighting of the terms. Unfortunately, networks trained this way only predict reasonable deformations for images with contrasts and shapes similar to the data observed during training. In our framework, we tackle this dependency.

3.2 Proposed method overview

We achieve contrast-invariance and robustness to anatomical variability by requiring no real training data, but instead synthesizing arbitrary contrasts and shapes through a generative process (Figure 3). We start from scratch, synthesizing two 3D paired label maps $\{s_m, s_f\}$ using a function $g_s(z) = \{s_m, s_f\}$ given random seed z . We then define the function $g_i(s_m, s_f, z) = \{m, f\}$ that synthesizes two 3D intensity volumes $\{m, f\}$ based on the maps $\{s_m, s_f\}$ and seed z .

This generative process resolves the limitations of existing methods as follows. First, training a registration network $h_\theta(m, f)$ using the generated images exposes it to arbitrary contrasts and shapes at each iteration, removing network dependency on specific modalities. Second, because we first synthesize label maps, we can use a similarity loss that measures label overlap independent of image contrast, thereby obviating the need for a cost function that depends on the contrasts being registered at that iteration. In our experiments, we use the (soft) Dice metric [47]

$$\mathcal{L}'_{dis}(\phi, s_m, s_f) = -\frac{2}{J} \sum_{j=1}^J \frac{|(s_m^j \circ \phi) \odot s_f^j|}{|(s_m^j \circ \phi) \oplus s_f^j|}, \quad (2)$$

where s^j represents the one-hot encoded label $j \in \{1, 2, \dots, J\}$ of label map s , and \odot and \oplus denote voxel-wise multiplication and addition, respectively.

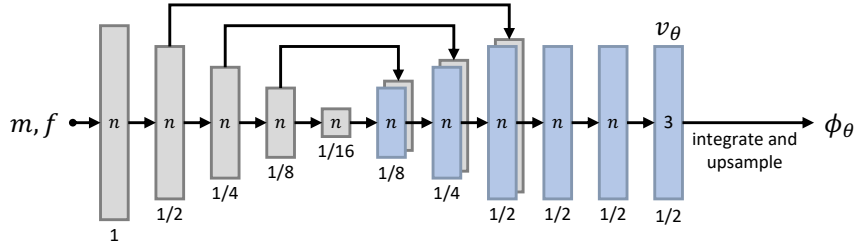


Figure 4: Convolutional U-Net architecture implementing $\phi_\theta = h_\theta(m, f)$. Each block of the encoder features a 3D convolution with $n=256$ filters and a LeakyReLU layer with parameter 0.2. The encoding stride-2 convolutions each halve the resolution relative to the input. In the decoder, each convolution is followed by an upsampling layer and a skip connection to the corresponding encoder block (indicated by long arrows). The SVF v_θ is obtained after three more convolutions at half resolution, yielding the deformation field ϕ_θ through integration and upsampling. All convolutional layers use $3 \times 3 \times 3$ kernels, and the final convolution leverages $n=3$ filters to bring v_θ to the desired shape.

Table 1: Hyperparameters. Spatial measures are given in voxels. In our experiments, images and label maps have a volume size of $160 \times 160 \times 192$. If fields are sampled at lower resolution r , the volume size is obtained by multiplying each dimension by r and rounding up (e.g. $4 \times 4 \times 5$ for $r = 1:40$).

Parameter	r_p	b_p	a_μ	b_μ	a_σ	b_σ	r_B	b_B	b_K	σ_γ	r_v	b_v
Value	1:32	100	25	225	5	25	1:40	0.3	1	0.25	1:16	2

While the framework can be used with any parametrization of the deformation field ϕ , in this work we use a stationary velocity field (SVF) v , which is integrated within the network to obtain a diffeomorphism [2, 3, 16], which is invertible by design. We regularize ϕ using $\mathcal{L}_{reg}(\phi) = \frac{1}{2} \|\nabla \mathbf{u}\|^2$, where \mathbf{u} is the displacement of deformation field $\phi = Id + \mathbf{u}$.

3.3 Generative model details

Label maps. To generate input label maps with J labels of random geometric shapes, we first draw J smoothly varying noise images p_j ($j \in \{1, 2, \dots, J\}$) by sampling voxels from a standard distribution at reduced resolution r_p and upsampling to full size (Figure 1). Second, each image p_j is warped with a random smooth deformation field ϕ_j (described below) to obtain images $\tilde{p}_j = p_j \circ \phi_j$. Third, we create an input label map s by assigning, for each voxel k of s , the label j among the images \tilde{p}_j that has the highest intensity, i.e. $s_k = \arg \max_j \{[\tilde{p}_j]_k\}$ (Figure 1).

Given a selected label map s , we generate two new label maps. First, we deform s with a random smooth diffeomorphic transformation ϕ_m (described below) using nearest-neighbor interpolation to produce the moving segmentation map $s_m = s \circ \phi_m$. An analogous process yields the fixed map s_f .

Alternatively, anatomical segmentations for the anatomy of interest can be used, for example from a public dataset. In this case, we select segmentation maps from two separate subjects at random and further deform them as described above (Figure 2). We emphasize that *no* acquired images, such as T1w or T2w MRI scans, are involved.

Synthetic images. From the pair of label maps $\{s_m, s_f\}$, we synthesize gray-scale images $\{m, f\}$ building on generative models of MR images used for Bayesian segmentation [4, 10, 65, 71, 77] (Figure 2). Given a segmentation map s , we draw the intensities of all image voxels that are associated with label j as independent samples from the normal distribution $\mathcal{N}(\mu_j, \sigma_j^2)$. We sample the mean μ_j and standard deviation (SD) σ_j for each label from continuous distributions $\mathcal{U}(a_\mu, b_\mu)$ and $\mathcal{U}(a_\sigma, b_\sigma)$, respectively, where a_μ, b_μ, a_σ , and b_σ are hyperparameters. To simulate partial volume effects [66], we convolve the image using an anisotropic Gaussian kernel $K(\sigma_{i=1,2,3})$ where $\sigma_{i=1,2,3} \sim \mathcal{U}(0, b_K)$.

We further corrupt the image with a spatially varying intensity-bias field B [8, 31]. We independently sample the voxels of B from a normal distribution $\mathcal{N}(0, \sigma_B^2)$ at reduced resolution r_B relative to the full image size (described below), where $\sigma_B \sim \mathcal{U}(0, b_B)$. We upsample B to full size, and take the exponential of each voxel to yield non-negative values before we apply B using element-wise multiplication. We obtain the final images m and f through min-max normalization and contrast augmentation through exponentiation, using the normally distributed parameter $\gamma \sim \mathcal{N}(0, \sigma_\gamma^2)$ such that $m = \tilde{m}^{\exp(\gamma)}$, where \tilde{m} is the normalized moving image, and similarly for the fixed image (Figure 2).

Random transforms. We obtain the transforms ϕ_j ($j = 1, 2, \dots, J$) for noise image p_j by integrating random SVFs v_j [2, 3, 16, 40]. We draw each voxel of v_j as an independent sample of a normal distribution $\mathcal{N}(0, \sigma_j^2)$ at reduced resolution r_p , where $\sigma_j \sim \mathcal{U}(0, b_p)$ is sampled uniformly, and each SVF is upsampled to full size. Analogous processes yield the transforms ϕ_m and ϕ_f based on hyperparameters r_v and b_v .

3.4 Implementation details

Hyperparameters. The generative process encompasses a number of parameters. During training, we sample these based on the hyperparameters presented in Table 1. Their values are *not* chosen to mimic realistic anatomy or a particular modality. Instead, we select hyperparameters visually to yield shapes and contrasts that far exceed the range of realistic medical images, to force the networks to

learn generalizable features that are independent of the characteristics of a specific modality [13]. We thoroughly analyze the impact of varying hyperparameters in our experiments.

Architecture. The network implementations follow the VoxelMorph architecture [6, 16]: a convolutional U-Net [57] predicts an SVF v_θ from the input $\{m, f\}$. As shown in Figure 4, the encoder has 4 blocks consisting of a stride-2 convolution and a LeakyReLU layer (parameter 0.2), that each halve the resolution relative to the inputs. The decoder features 3 blocks that each include a stride-1 convolution, an upsampling layer and a skip connection to the corresponding encoder block. We obtain the SVF v_θ after 3 further convolutions at half resolution, and the deformation ϕ_θ after integration and upsampling. All convolutional layers in the network use $n=256$ filters of size $3 \times 3 \times 3$, except for the last one ($n=3$).

Implementation. Networks are implemented using Keras [15] with a TensorFlow backend [1]. We use a GPU version [16, 40] of *scaling and squaring* with 5 steps to integrate SVFs [2, 3].

4 Experiments

We evaluate several variants of the proposed registration network and compare its performance to a set of baselines. The datasets include a variety of image contrasts and levels of processing to assess method robustness. Our main goal is for SynthMorph to generalize well to unseen real contrasts during rapid test time registration, while matching or exceeding the accuracy of classical methods, or learning methods tested on the same data type they were trained on.

4.1 Experimental setup

Data. We compile 3D brain-MRI datasets from the Human Connectome Aging Project (HCP-A) [11, 27] and the Alzheimer’s Disease Neuroimaging Initiative (ADNI) [70]. HCP-A includes T1w MPRAGE [49] and T2w T2SPACE scans of the same subjects without preprocessing. ADNI includes T1w gradient-unwarped and bias-field corrected MPRAGE scans. We also use skullstripped in-house PDw scans from 8 subjects. For image synthesis for one model variant, we use 40 label maps from distinct-subject MPRAGE scans of the Buckner40 dataset [22]. Brain and non-brain labels for skullstripping, image synthesis and evaluation are derived using SAMSEG [50], except for the PDw data, which include manual maps. As we focus on deformable registration, all images are mapped to a common affine space [21, 53] at 1 mm isotropic resolution.

Setup. For each contrast, we run experiments on 30 image pairs, where each image is from a different subject, except for T1-PD pairs, of which we have only 8. To assess robustness to non-brain structures, we evaluate registration within and across datasets, with and without skull-stripping, using additional held-out datasets of the same size.

Baselines. We test classical registration with ANTs (SyN) [5] using default parameters [51] for the NCC similarity metric within contrast, and MI across contrasts. We test NiftyReg [48] with default cost function (NMI) and parameters and enable its diffeomorphic model with SVF integration as in our approach. Both ANTs and NiftyReg focus on neuroimaging, leading to appropriate default parameters for our tasks. We also run the deedsBCV patch-similarity method, which we tune for neuroimaging. To match the spatial scales of brain structures, we reduce the default grid spacing, search radius and quantization step to $6 \times 5 \times 4 \times 3 \times 2$, $6 \times 5 \times 4 \times 3 \times 2$ and $5 \times 4 \times 3 \times 2 \times 1$, respectively, which improves registration in our experiments.

As a learning baseline, we train VoxelMorph (vm), using the same architecture as SynthMorph but with NCC, on 100 skull-stripped T1w HCP-A images that do not overlap with validation data, and another model trained with NMI on random combinations of 100 T1w and 100 T2w images (including e.g. T2w-T2w pairs).

SynthMorph variants. For imaging-data and shape-agnostic training, we sample $\{s_m, s_f\}$ from one of 100 random-shape segmentations s at each iteration (sm-shapes). Each s contains $J=26$ labels that we all include in the loss \mathcal{L}_{dis} . Since brain segmentations are often available, even if not for the target modality, we also test our framework when starting with a set of brain-anatomy label maps (sm-brains). In this case, we sample $\{s_m, s_f\}$ from two distinct maps at each iteration and further deform these label maps using synthetic warps. The segmentations include non-brain labels,

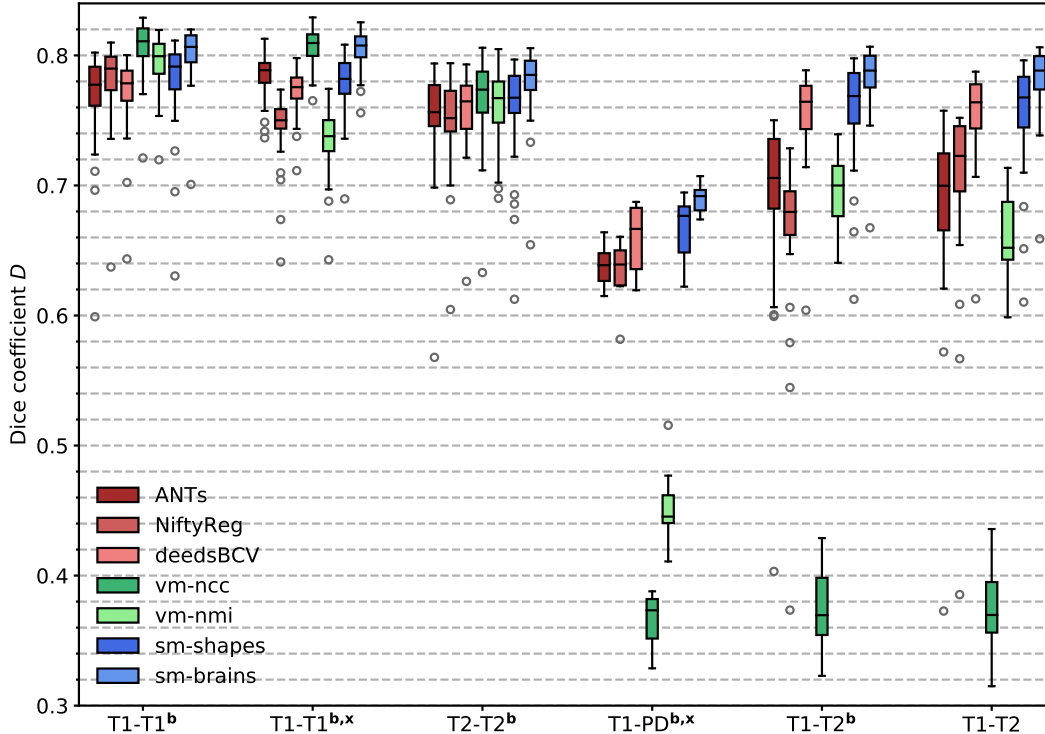


Figure 5: Registration accuracy. Each box shows overlap of anatomical structures for 30 test-image pairs across distinct subjects (8 when using PD contrast). The letters **b** and **x** indicate skullstripped data and registration across datasets (e.g. between ADNI and HCP-A), respectively.

and we optimize the $J=26$ largest brain labels in \mathcal{L}_{dis} (see below). We emphasize that no real images are used during SynthMorph training.

Assessment. We measure registration accuracy using the Dice metric D [19] across a representative subset of brain structures: amygdala, brainstem, caudate, ventral DC, cerebellar white matter and cortex, pallidum, cerebral white matter (WM) and cortex, hippocampus, lateral ventricle, putamen, thalamus, 3rd and 4th ventricle, and choroid-plexus. Bilateral structure scores are averaged. We also compute the proportion of voxels where the deformation ϕ folds, i.e. with $\det(J_\phi) \leq 0$ for voxel Jacobian J_ϕ .

Framework analysis. To evaluate network invariance to realistic MRI contrast, we perform the following procedure for 10 subject pairs. We obtain 8 spoiled gradient-echo [12] images for the same brain, progressing from T1w to PDw as shown in Figure 7, using Bloch equation simulations with acquired parametric maps (T1, T2*, PD). We run a separate registration between each contrast and the most T1w-like of another subject, and analyze the variation of the features of the last network layer (before the SVF is formed). Specifically, we compute the root-mean-square difference d (RMSD) between the layer outputs of the first and each other contrast over space, averaged over contrasts, features, and subjects. Original MRI sequence details are: spoiled gradient-echo, 2 ms echo time (TE), 20 ms repetition time (TR), 2-40° flip angle (FA).

In a validation set, we explore the effect of various hyperparameters. First, we train with regularization weights $\lambda \in [0, 10]$ and evaluate accuracy across: (1) all brain labels, (2) only the largest 26 (bilateral) structures optimized in \mathcal{L}_{dis} . Second, we train variants of our model with varied deformation range b_v , image smoothness b_K , and number of features n per layer. Third, for the case that brain segmentations are available, we analyze the effect of training with (1) full-head labels, (2) brain labels only or (3) a mixture of both.

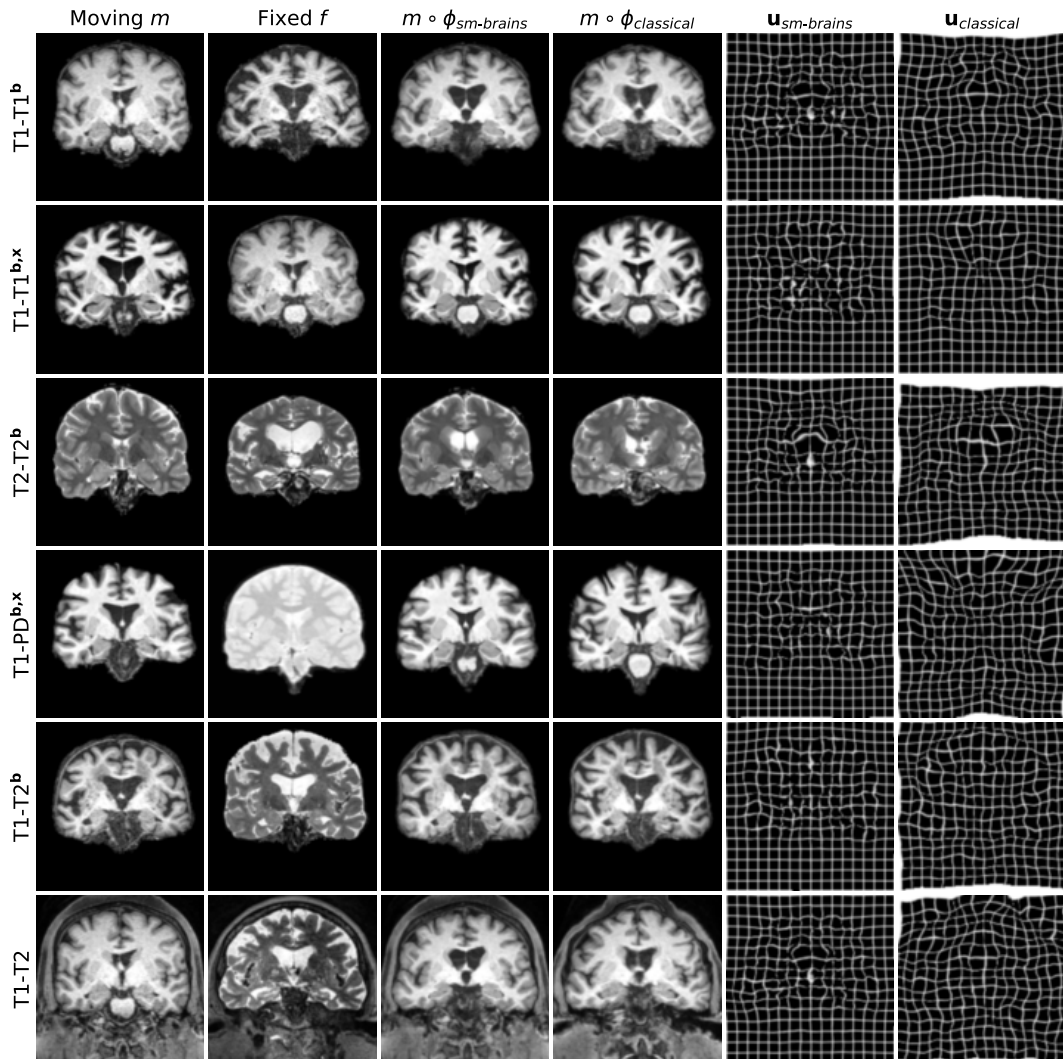


Figure 6: Typical registration results for SynthMorph (sm-brains) and classical methods. Each row shows a registration pair from the source datasets indicated on the left, where the letters **b** and **x** mark skullstripped data and registration across datasets (e.g. between ADNI and HCP-A), respectively. For each dataset, we show the best-performing classical baseline: NiftyReg on the 1st, ANTs on the 2nd, and deedsBCV on all other rows.

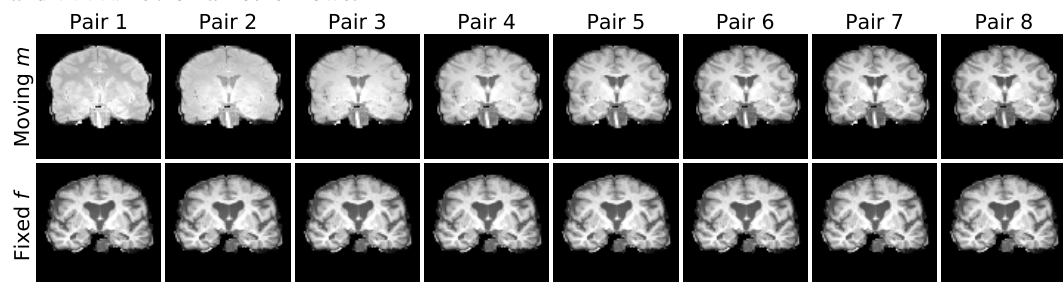


Figure 7: MRI contrasts used to assess network invariance. We obtain images with real MR contrasts progressing from proton-density (PD, top left) to T1-weighted for the same brain using Bloch-equation simulations with acquired parametric maps (T1, T2*, PD). For each subject pair, we compile and illustrate 8 contrasts.

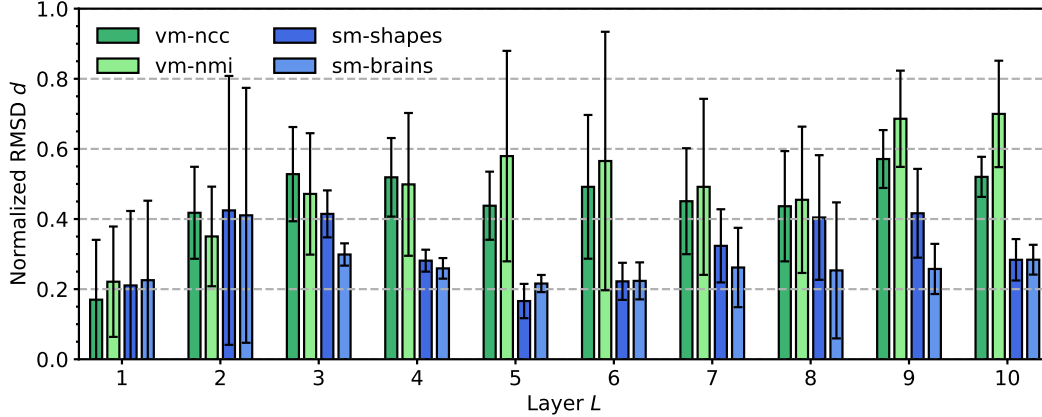


Figure 8: Variability of network layers in response to 10 realistic MRI-contrast pairs from distinct subjects as shown in Figure 7. We use normalized root-mean-square deviation (RMSD) d between each contrast and the most T1w-like, averaged over contrasts, features, and subjects. For the analysis, networks use the same architecture with $n=64$ filters per convolutional layer. Error bars indicate standard deviation across features.

4.2 Results

Typical registration results are shown in Figure 6. Figure 5 compares mean Dice scores across structures for all methods, while Figure 12 shows scores for individual structures. By exploiting the anatomical information in a set of brain labels, *sm-brains* achieves the best accuracy across all datasets, even though no real images are used during training. First, *sm-brains* outperforms classical methods on all tasks by at least 2 Dice points, and often much more ($p < 0.04$ for T1-PD, $p < 5 \times 10^{-8}$ for all other tasks). Second, it matches the state-of-the-art accuracy of *vm-ncc* for T1-T1 registration, which was trained on real T1 images. Across contrasts, *sm-brains* outperforms all other methods by 3 or more Dice points, demonstrating its ability to generalize to contrasts, compared especially to the baseline learning methods which cannot generalize to contrast unseen during training.

The shape and contrast agnostic network *sm-shapes* matches the performance of the best classical method for each dataset except T1-T1 registration, where it slightly underperforms, despite never having been exposed to either imaging data or even brain anatomical shapes. Like *sm-brains*, *sm-shapes* generalizes well to multi-contrast registration, matching or exceeding the accuracy of all baselines.

The baseline learning methods *vm-ncc* and *vm-nmi* perform well and clearly outperform classical methods when faced with contrasts similar to those used in training. However, as expected, these approaches break down when tested on a pair of new contrasts.

In our experiments, learning-based models require less than 1 second per 3D registration on an Nvidia Tesla V100 GPU. Using default settings, *NiftyReg* and *ANTs* typically take ~ 0.5 h and ~ 1.2 h on a 3.3-GHz Intel Xeon CPU (single-threaded), respectively, whereas *deedsBCV* typically requires ~ 3 min.

4.3 Analyses

Figure 8 illustrates the variability of the response of each network layer to varying MRI contrast of the same anatomy shown in Figure 7. Figure 9 contains example feature maps. *SynthMorph* models exhibit substantially less variability than baseline learning models for each feature, indicating that the proposed strategy encourages contrast-invariance.

Figure 10 shows registration performance for various training settings. For *sm-brains*, best results are obtained with low deformation strength b_v , when label maps s from two different subjects are used at each iteration (Figure 10A). A larger value of $b_v=2$ is optimal for *sm-shapes*, for which $\{s_m, s_f\}$ are generated from a single s , thus lacking the inter-subject deformation.

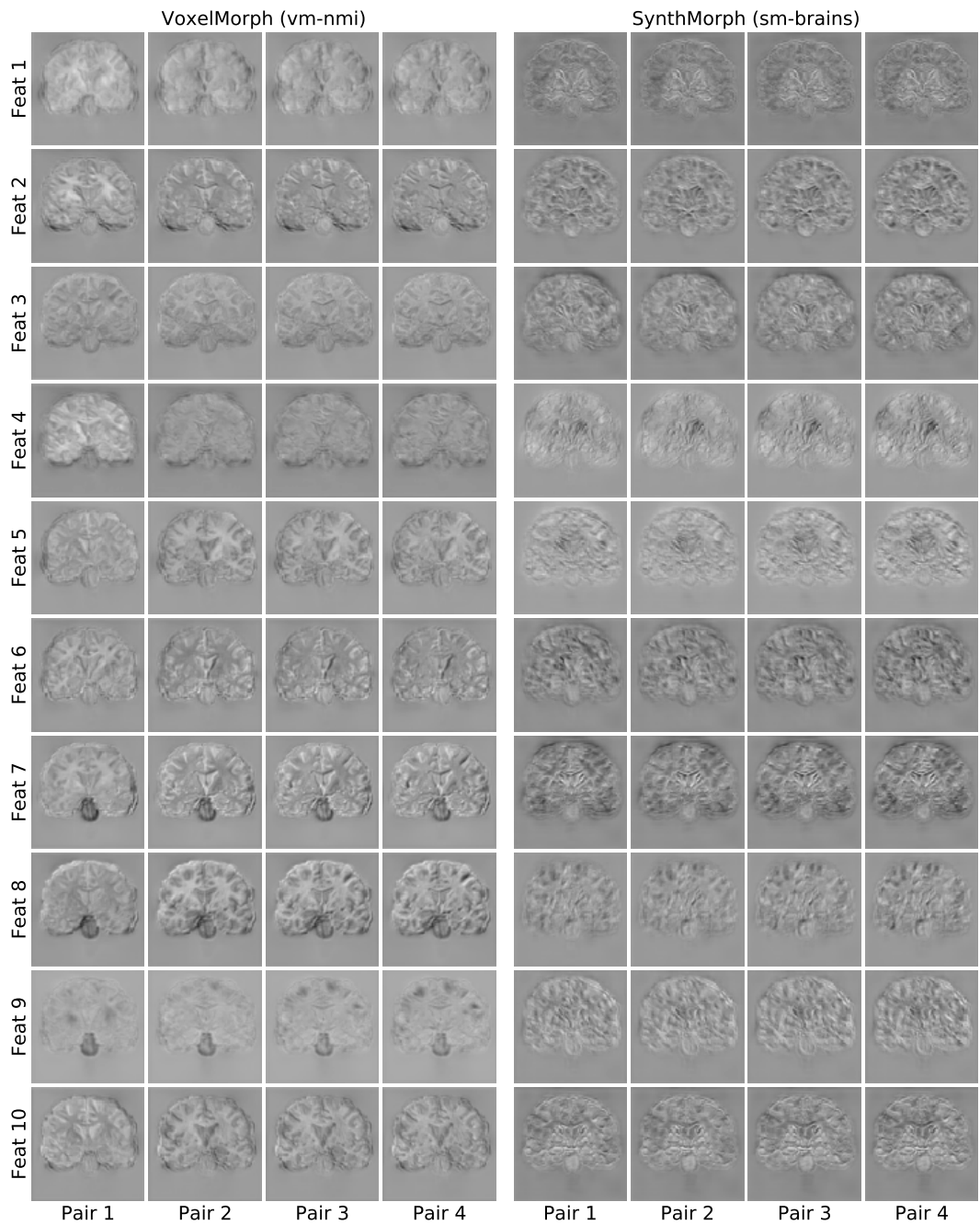


Figure 9: Representative features of the last network layer (before forming the SVF) in response to the realistic MRI-contrast pairs shown in Figure 7. Left: VoxelMorph using normalized mutual information (NMI), exhibiting variability among contrasts. Right: contrast-invariant SynthMorph (sm-brains). For the analysis, both networks use the same architecture with $n=64$ filters per convolutional layer.

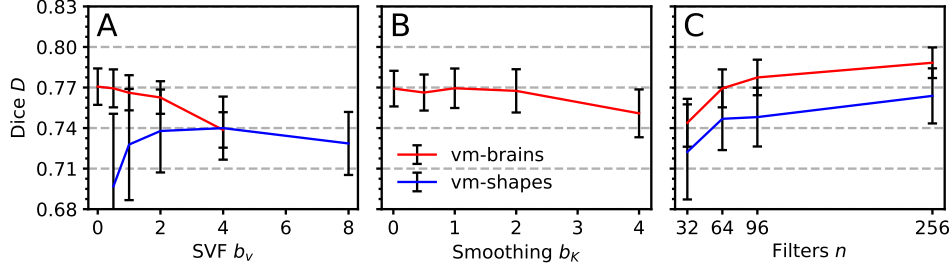


Figure 10: Framework analysis showing the effect of training settings on registration accuracy: **A.** Maximum velocity-field SD b_v . **B.** Maximum image-smoothing SD b_K . **C.** Number of filters n per convolutional layer.

Random blurring of the images $\{m, f\}$ improves robustness to data with different smoothing levels, with optimal accuracy at $b_K=1$ (Figure 10B). Higher numbers of filters n per convolutional layer boost the accuracy at the cost of increasing training times from days to weeks (Figure 10C), indicating that richer networks are better able to capture and generalize from synthesized data. Finally, training on full-head as compared to skull-stripped images had little impact on accuracy (not shown).

Figure 11A shows that with reducing regularization, accuracy increases for the large structures used in \mathcal{L}_{dis} . When we include smaller structures, the mean overlap D reduces for $\lambda < 1$, as the network then focuses on optimizing the training structures. This does not apply to `sm-shapes`, which is agnostic to anatomy and trained on all synthetic labels present in the random maps. Figure 11B shows a small proportion of locations where the warp field folds, decreasing with increasing λ . For test results, we use a value of $\lambda = 1$, where the proportion of folding voxels is $\sim 10^{-6}$ at our numerical precision. Unless indicated, all hyperparameters are tested using $n=64$ convolutional filters per layer to enable analysis.

5 Conclusion

We propose SynthMorph, an unsupervised learning framework for modality-invariant image registration, training networks with samples of a generative model with widely varying synthetic contrast and shape. In our experiments, we find SynthMorph variants to achieve registration accuracy matching or outperforming classical methods, and are significantly faster. If brain labels are available, they enable even further improvement. While learning-based methods like `VoxelMorph` yield results comparable to `sm-brains` for contrasts observed during training, they break down when presented with other contrasts, whereas SynthMorph remains robust.

A significant challenge in deployment of neural networks is their generalizability. SynthMorph performance is achieved although our network does not have access to the contrasts present in the test set, nor indeed to any real MRI data, obviating the need for re-training for a new modality. We empirically observe this invariance directly by examining network channel outputs. We therefore

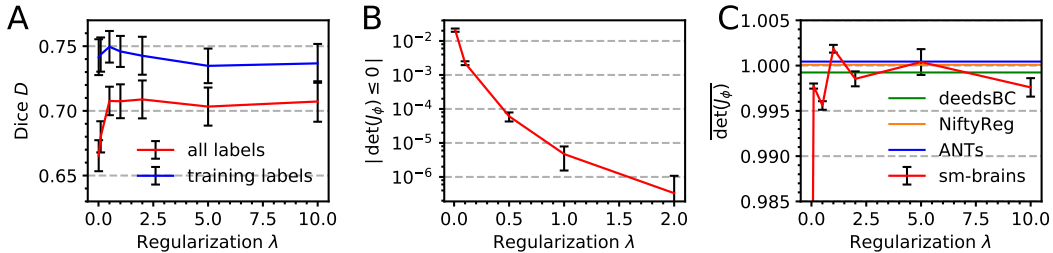


Figure 11: Regularization analysis. **A** Registration accuracy. **B** Proportion of locations where the deformation field ϕ folds, i.e. with a Jacobian J_ϕ such that $\det(J_\phi) \leq 0$ (of 4.9×10^6 voxels). **C** Average Jacobian determinant. For $\lambda \geq 1$, the deviation from the the ideal value 1 is below 2×10^{-3} .

believe this strategy can be broadly applied to registration networks to limit the need for training data while simultaneously improving applicability.

While the proposed technique addresses important drawbacks of classical and learning-based methods for within and across contrast registration, it can be expanded in several ways. Since some data is often available at training, we will investigate whether combining real images and synthetic data might improve registration accuracy in popular use cases, while maintaining invariance to *unseen* data. Combining our training loss with classical cost functions may also improve accuracy providing better signal in label interiors. Finally, while we are focused on neuroimaging, this approach promises to be extensible to images of other body parts, and may eventually lead to a single registration model that can accurately align unprocessed images of any modality and body part, or even outside medical imaging.

Broader impact

Any image registration algorithm that depends on a collection of images can be biased by the demographic makeup of the available subjects. For example, concerns have been expressed in the neuroimaging community that atlases used to instantiate a reference coordinate system are ripe for bias due to the relatively homogeneous subject populations used to construct them.

In this work we focus on the development of a general-purpose tool for nonlinear contrast-agnostic (e.g. T1w-to-PDw MRI) registration to fill an unmet need in medical imaging. We achieve this via two approaches: first, using brain label maps (no images) that are then warped based on deformations that are substantially more extreme than what is seen in the real world, and second, using no real data but instead training a network with labels and images generated purely from noise. We believe that these approaches have technical promise, and, from a societal perspective, can considerably reduce bias by eliminating the need for any training population and hence a potentially biased demographic sample.

For proper deployment, the framework needs to be evaluated thoroughly, including the range of geometric and imaging features that are important in the safe generalizability of such networks. Because the method presents a new training paradigm, it needs to be analyzed on a representative, broad set of imaging data to ensure consistent results across patient demographic as well as anatomical and pathological variability. Although more research is needed for safe deployment, we believe these approaches hold promise in providing fair and impartial algorithms.

Finally, we also hope that the method will eliminate the need to acquire large datasets for registering a particular modality, relieving environmental burdens, due to technologies involved in acquisition, and scientific/societal burdens, as it has the potential to free researchers from both extra acquisitions and manually labeling those data for evaluation or training.

Acknowledgments

This research was supported by the European Research Council (ERC Starting Grant 677697, project BUNGEE-TOOLS), and by the National Institutes of Health (NIH) grant U01-AG052564.

Further support was provided in part by the BRAIN Initiative Cell Census Network grant U01-MH117023, the National Institute for Biomedical Imaging and Bioengineering (P41-EB015896, 1R01-EB023281, R01-EB006758, R21-EB018907, R01-EB019956), the National Institute on Aging (1R56-AG064027, 1R01-AG064027, 5R01-AG008122, R01-AG016495), the National Institute of Mental Health the National Institute of Diabetes and Digestive and Kidney Diseases (1-R21-DK-108277-01), the National Institute for Neurological Disorders and Stroke (R01-NS0525851, R21-NS072652, R01-NS070963, R01-NS083534, 5U01-NS086625, 5U24-NS10059103, R01-NS105820). The project also benefited from the resources provided by Shared Instrumentation Grants 1S10-RR023401, 1S10-RR019307, and 1S10-RR023043. Additional support was provided by the NIH Blueprint for Neuroscience Research (5U01-MH093765), part of the multi-institutional Human Connectome Project. BF has a financial interest in CorticoMetrics, a company focusing on brain imaging and measurement technologies. BF's interests were reviewed and are managed by Massachusetts General Hospital and Partners HealthCare in accordance with their conflict of interest policies.

References

- [1] Martín Abadi, Paul Barham, Jianmin Chen, Zhifeng Chen, Andy Davis, Jeffrey Dean, et al. Tensorflow: A system for large-scale machine learning. In *12th USENIX Symposium on Operating Systems Design and Implementation (OSDI)*, pages 265–283, 2016.
- [2] Vincent Arsigny, Olivier Commowick, Xavier Pennec, and Nicholas Ayache. A log-euclidean framework for statistics on diffeomorphisms. In *MICCAI*, pages 924–931. Springer, 2006.
- [3] John Ashburner. A fast diffeomorphic image registration algorithm. *Neuroimage*, 38(1):95–113, 2007.
- [4] John Ashburner and Karl J Friston. Unified segmentation. *Neuroimage*, 26:839–851, 2005.
- [5] B.B. Avants, C.L. Epstein, M. Grossman, and J.C. Gee. Symmetric diffeomorphic image registration with cross-correlation: Evaluating automated labeling of elderly and neurodegenerative brain. *Medical Image Analysis*, 12(1):26 – 41, 2008.
- [6] Guha Balakrishnan, Amy Zhao, Mert Sabuncu, John Guttag, and Adrian V. Dalca. Voxelmorph: A learning framework for deformable medical image registration. *IEEE Trans. Med. Im.*, 38(8):1788–00, 2019.
- [7] M Faisal Beg, Michael I Miller, Alain Trouvé, and Laurent Younes. Computing large deformation metric mappings via geodesic flows of diffeomorphisms. *International journal of computer vision*, 61(2):139–157, 2005.
- [8] Boubakeur Belaroussi, Julien Milles, Sabin Carme, Yue Min Zhu, and Hugues Benoit-Cattin. Intensity non-uniformity correction in mri: existing methods and their validation. *Medical image analysis*, 10(2):234–246, 2006.
- [9] Chitresh Bhushan, Justin P Haldar, Soyoung Choi, Anand A Joshi, David W Shattuck, and Richard M Leahy. Co-registration and distortion correction of diffusion and anatomical images based on inverse contrast normalization. *Neuroimage*, 115:269–280, 2015.
- [10] Benjamin Billot, Douglas Greve, Koen Van Leemput, Bruce Fischl, Juan Eugenio Iglesias, and Adrian V Dalca. A learning strategy for contrast-agnostic mri segmentation. *arXiv preprint arXiv:2003.01995*, 2020.
- [11] Susan Y. Bookheimer, David H. Salat, Melissa Terpstra, Beau M. Ances, Deanna M. Barch, Randy L. Buckner, Gregory C. Burgess, et al. The lifespan human connectome project in aging: An overview. *NeuroImage*, 185:335 – 348, 2019.
- [12] Richard B Buxton, Robert R Edelman, Bruce R Rosen, Gary L Wismer, and Thomas J Brady. Contrast in rapid mr imaging: T1- and t2-weighted imaging. *Journal of computer assisted tomography*, 11(1):7–16, 1987.
- [13] Krishna Chaitanya, Neerav Karani, Christian F Baumgartner, Anton Becker, Olivio Donati, and Ender Konukoglu. Semi-supervised and task-driven data augmentation. In *IPMI*, pages 29–41. Springer, 2019.
- [14] Min Chen, Aaron Carass, Amod Jog, Junghoon Lee, Snehashis Roy, and Jerry L Prince. Cross contrast multi-channel image registration using image synthesis for mr brain images. *Medical image analysis*, 36:2–14, 2017.
- [15] François Chollet. Keras: The python deep learning library, 2015.
- [16] Adrian V. Dalca, Guha Balakrishnan, John Guttag, and Mert Sabuncu. Unsupervised learning of probabilistic diffeomorphic registration for images and surfaces. *Medical Image Analysis*, 57:226–236, 2019.
- [17] Bob D de Vos, Floris F Berendsen, Max A Viergever, Hessam Sokooti, Marius Staring, and Ivana Išgum. A deep learning framework for unsupervised affine and deformable image registration. *Medical image analysis*, 52:128–143, 2019.
- [18] Bob D de Vos, Floris F Berendsen, Max A Viergever, Marius Staring, and Ivana Išgum. End-to-end unsupervised deformable image registration with a convolutional neural network. In *Deep Learning in Medical Image Analysis and Multimodal Learning for Clinical Decision Support*, pages 204–212. Springer, 2017.
- [19] Lee R Dice. Measures of the amount of ecologic association between species. *Ecology*, 26(3):297–302, 1945.

- [20] K. A. J. Eppenhof and J. P. W. Pluim. Pulmonary ct registration through supervised learning with convolutional neural networks. *IEEE Transactions on Medical Imaging*, 38(5):1097–1105, 2019.
- [21] Bruce Fischl. Freesurfer. *NeuroImage*, 62(2):774 – 781, 2012. 20 YEARS OF fMRI.
- [22] Bruce Fischl, David H Salat, Evelina Busa, Marilyn Albert, Megan Dieterich, Christian Haselgrove, et al. Whole brain segmentation: automated labeling of neuroanatomical structures in the human brain. *Neuron*, 33(3):341–355, 2002.
- [23] R.S.J. Frackowiak, K.J. Friston, C. Frith, R. Dolan, C.J. Price, S. Zeki, J. Ashburner, and W.D. Penny. *Human Brain Function*. Academic Press, 2nd edition, 2003.
- [24] Christoph Guetter, Chenyang Xu, Frank Sauer, and Joachim Hornegger. Learning based non-rigid multi-modal image registration using kullback-leibler divergence. In *International Conference on Medical Image Computing and Computer-Assisted Intervention*, pages 255–262. Springer, 2005.
- [25] Courtney K Guo. *Multi-modal image registration with unsupervised deep learning*. PhD thesis, Massachusetts Institute of Technology, 2019.
- [26] Eldad Haber and Jan Modersitzki. Intensity gradient based registration and fusion of multi-modal images. In *International Conference on Medical Image Computing and Computer-Assisted Intervention*, pages 726–733. Springer, 2006.
- [27] Michael P. Harms, Leah H. Somerville, Beau M. Ances, Jesper Andersson, Deanna M. Barch, et al. Extending the human connectome project across ages: Imaging protocols for the lifespan development and aging projects. *NeuroImage*, 183:972 – 984, 2018.
- [28] Mattias P. Heinrich, Mark Jenkinson, Manav Bhushan, Tahreema Matin, Fergus V. Gleeson, Sir Michael Brady, and Julia A. Schnabel. Mind: Modality independent neighbourhood descriptor for multi-modal deformable registration. *Medical Image Analysis*, 16(7):1423 – 1435, 2012. Special Issue on the 2011 Conference on Medical Image Computing and Computer Assisted Intervention.
- [29] Mattias P. Heinrich, Ivor J.A. Simpson, BartŁomiej W. Papież, Sir Michael Brady, and Julia A. Schnabel. Deformable image registration by combining uncertainty estimates from supervoxel belief propagation. *Medical Image Analysis*, 27:57 – 71, 2016. Discrete Graphical Models in Biomedical Image Analysis.
- [30] Alessa Hering, Sven Kuckertz, Stefan Heldmann, and Mattias P Heinrich. Enhancing label-driven deep deformable image registration with local distance metrics for state-of-the-art cardiac motion tracking. In *Bildverarbeitung für die Medizin 2019*, pages 309–314. Springer, 2019.
- [31] Zujun Hou. A review on mr image intensity inhomogeneity correction. *International journal of biomedical imaging*, 2006, 2006.
- [32] Yipeng Hu, Marc Modat, Eli Gibson, Nooshin Ghavami, Ester Bonmati, Caroline M Moore, Mark Emberton, J Alison Noble, Dean C Barratt, and Tom Vercauteren. Label-driven weakly-supervised learning for multimodal deformable image registration. In *2018 IEEE 15th International Symposium on Biomedical Imaging (ISBI 2018)*, pages 1070–1074. IEEE, 2018.
- [33] Yipeng Hu, Marc Modat, Eli Gibson, Wenqi Li, Nooshin Ghavami, Ester Bonmati, Guotai Wang, Steven Bandula, Caroline M Moore, Mark Emberton, et al. Weakly-supervised convolutional neural networks for multimodal image registration. *Medical image analysis*, 49:1–13, 2018.
- [34] Juan Eugenio Iglesias, Ender Konukoglu, Darko Zikic, Ben Glocker, Koen Van Leemput, and Bruce Fischl. Is synthesizing mri contrast useful for inter-modality analysis? In *MICCAI*, pages 631–638. Springer, 2013.
- [35] Konstantinos Kamnitsas, Christian Baumgartner, Christian Ledig, Virginia Newcombe, Joanna Simpson, Andrew Kane, David Menon, Aditya Nori, et al. Unsupervised domain adaptation in brain lesion segmentation with adversarial networks. In *IPMI*, pages 597–609, 2017.
- [36] Fahdi Kanavati, Tong Tong, Kazunari Misawa, Michitaka Fujiwara, Kensaku Mori, Daniel Rueckert, and Ben Glocker. Supervoxel classification forests for estimating pairwise image correspondences. *Pattern Recognition*, 63:561 – 569, 2017.
- [37] Arno Klein, Jesper Andersson, Babak A Ardekani, John Ashburner, Brian Avants, Ming-Chang Chiang, et al. Evaluation of 14 nonlinear deformation algorithms applied to human brain MRI registration. *Neuroimage*, 46(3):786–802, 2009.

- [38] Lars König, Alexander Derksen, Marc Hallmann, and Nils Papenberg. Parallel and memory efficient multimodal image registration for radiotherapy using normalized gradient fields. In *2015 IEEE 12th international symposium on biomedical imaging (ISBI)*, pages 734–738. IEEE, 2015.
- [39] Lars König and Jan Rühaak. A fast and accurate parallel algorithm for non-linear image registration using normalized gradient fields. In *2014 IEEE 11th international symposium on biomedical imaging (ISBI)*, pages 580–583. IEEE, 2014.
- [40] Julian Krebs, Hervé Delingette, Boris Mailhé, Nicholas Ayache, and Tommaso Mansi. Learning a probabilistic model for diffeomorphic registration. *IEEE TMI*, 38(9):2165–2176, 2019.
- [41] Julian Krebs, Tommaso Mansi, Hervé Delingette, Li Zhang, Florin Ghesu, et al. Robust non-rigid registration through agent-based action learning. In *MICCAI*, pages 344–352, 2017.
- [42] Hongming Li and Yong Fan. Non-rigid image registration using fully convolutional networks with deep self-supervision. *arXiv preprint arXiv:1709.00799*, 2017.
- [43] M. Lorenzi, N. Ayache, G.B. Frisoni, and X. Pennec. Lcc-demons: A robust and accurate symmetric diffeomorphic registration algorithm. *NeuroImage*, 81:470 – 483, 2013.
- [44] Lucas Mansilla, Diego H Milone, and Enzo Ferrante. Learning deformable registration of medical images with anatomical constraints. *Neural Networks*, 124:269–279, 2020.
- [45] Donald W McRobbie, Elizabeth A Moore, Martin J Graves, and Martin R Prince. *MRI from Picture to Proton*. Cambridge university press, 2017.
- [46] Matthew Mellor and Michael Brady. Phase mutual information as a similarity measure for registration. *Medical image analysis*, 9(4):330–343, 2005.
- [47] Fausto Milletari, Nassir Navab, and Seyed-Ahmad Ahmadi. V-net: Fully convolutional neural networks for volumetric medical image segmentation. In *2016 3DV*, pages 565–571, 2016.
- [48] Marc Modat, Gerard R. Ridgway, Zeike A. Taylor, Manja Lehmann, Josephine Barnes, David J. Hawkes, et al. Fast free-form deformation using graphics processing units. *Computer Methods and Programs in Biomedicine*, 98(3):278 – 284, 2010. HP-MICCAI 2008.
- [49] John P Mugler III and James R Brookeman. Three-dimensional magnetization-prepared rapid gradient-echo imaging (3d mp rage). *MRM*, 15(1):152–157, 1990.
- [50] Oula Puonti, Juan Eugenio Iglesias, and Koen Van Leemput. Fast and sequence-adaptive whole-brain segmentation using parametric bayesian modeling. *NeuroIm.*, 143:235–249, 2016.
- [51] Dorian Pustina and Philip Cook. Anatomy of an antsregistration call, 2017.
- [52] Chen Qin, Bibo Shi, Rui Liao, Tommaso Mansi, Daniel Rueckert, and Ali Kamen. Unsupervised deformable registration for multi-modal images via disentangled representations. In *IPMI*, pages 249–261. Springer, 2019.
- [53] Martin Reuter, H. Diana Rosas, and Bruce Fischl. Highly accurate inverse consistent registration: A robust approach. *NeuroImage*, 53(4):1181 – 1196, 2010.
- [54] Alexis Roche, Grégoire Malandain, Xavier Pennec, and Nicholas Ayache. The correlation ratio as a new similarity measure for multimodal image registration. *MICCAI*, pages 1115–24, 1998.
- [55] Marc Rohé, Manasi Datar, Tobias Heimann, Maxime Sermesant, and Xavier Pennec. SVF-Net: Learning deformable image registration using shape matching. *MICCAI*, pages 266–274, 2017.
- [56] Karl Rohr, H Siegfried Stiehl, Rainer Sprengel, Thorsten M Buzug, Jürgen Weese, and MH Kuhn. Landmark-based elastic registration using approximating thin-plate splines. *IEEE TMI*, 20(6):526–534, 2001.
- [57] Olaf Ronneberger, Philipp Fischer, and Thomas Brox. U-net: Convolutional networks for biomedical image segmentation. *CoRR*, abs/1505.04597, 2015.
- [58] Snehashis Roy, Aaron Carass, Amod Jog, Jerry L Prince, and Junghoon Lee. Mr to ct registration of brains using image synthesis. In *Medical Imaging 2014: Image Processing*, volume 9034, page 903419. International Society for Optics and Photonics, 2014.
- [59] Daniel Rueckert, Luke I Sonoda, Carmel Hayes, Derek LG Hill, Martin O Leach, and David J Hawkes. Nonrigid registration using free-form deformations: application to breast mr images. *IEEE TMI*, 18(8):712–721, 1999.

- [60] Jan Rühaak, Lars König, Marc Hallmann, Nils Papenberg, Stefan Heldmann, Hanno Schumacher, and Bernd Fischer. A fully parallel algorithm for multimodal image registration using normalized gradient fields. In *2013 IEEE 10th International Symposium on Biomedical Imaging*, pages 572–575. IEEE, 2013.
- [61] Hessam Sokooti, Bob de Vos, Floris Berendsen, Boudewijn PF Lelieveldt, Ivana Išgum, and Marius Staring. Nonrigid image registration using multi-scale 3d convolutional neural networks. In *MICCAI*, pages 232–239. Springer, 2017.
- [62] Ramesh Sridharan, Adrian V Dalca, Kaitlin M Fitzpatrick, Lisa Cloonan, Allison Kanakis, Ona Wu, Karen L Furie, Jonathan Rosand, Natalia S Rost, and Polina Golland. Quantification and analysis of large multimodal clinical image studies: Application to stroke. In *International Workshop on Multimodal Brain Image Analysis*, pages 18–30. Springer, 2013.
- [63] Christine Tanner, Firat Ozdemir, Romy Profanter, Valeriy Vishnevsky, Ender Konukoglu, and Orcun Goksel. Generative adversarial networks for mr-ct deformable image registration. *arXiv preprint arXiv:1807.07349*, 2018.
- [64] Bram van Ginneken, Sjoerd Kerkstra, and James Meakin. Miccai challenge 2019 for correction of brain shift with intra-operative ultrasound (curious 2019), 2019.
- [65] Koen Van Leemput, Frederik Maes, Dirk Vandermeulen, and Paul Suetens. Automated model-based tissue classification of mr images of the brain. *IEEE TMI*, 18:897–908, 1999.
- [66] Koen Van Leemput, Frederik Maes, Dirk Vandermeulen, and Paul Suetens. A unifying framework for partial volume segmentation of brain mr images. *IEEE transactions on medical imaging*, 22(1):105–119, 2003.
- [67] Tom Vercauteren, Xavier Pennec, Aymeric Perchant, and Nicholas Ayache. Diffeomorphic demons: Efficient non-parametric image registration. *NeuroImage*, 45(1):S61–S72, 2009.
- [68] Paul Viola and William M Wells III. Alignment by maximization of mutual information. *International journal of computer vision*, 24(2):137–154, 1997.
- [69] Christian Wachinger and Nassir Navab. Entropy and laplacian images: Structural representations for multi-modal registration. *Medical image analysis*, 16(1):1–17, 2012.
- [70] Michael W Weiner. Alzheimer’s disease neuroimaging initiative (ADNI) database, 2003.
- [71] William M Wells, W Eric L Grimson, Ron Kikinis, and Ferenc A Jolesz. Adaptive segmentation of mri data. *IEEE transactions on medical imaging*, 15(4):429–442, 1996.
- [72] Guorong Wu, Minjeong Kim, Qian Wang, Brent C Munsell, and Dinggang Shen. Scalable high-performance image registration framework by unsupervised deep feature representations learning. *IEEE Transactions on Biomedical Engineering*, 63(7):1505–1516, 2015.
- [73] Junshen Xu, Molin Zhang, Esra Abaci Turk, Larry Zhang, P Ellen Grant, Kui Ying, Polina Golland, and Elfar Adalsteinsson. Fetal pose estimation in volumetric mri using a 3d convolution neural network. In *MICCAI*, pages 403–410. Springer, 2019.
- [74] Z. Xu, C. P. Lee, M. P. Heinrich, M. Modat, D. Rueckert, S. Ourselin, R. G. Abramson, and B. A. Landman. Evaluation of six registration methods for the human abdomen on clinically acquired ct. *IEEE Transactions on Biomedical Engineering*, 63(8):1563–1572, 2016.
- [75] Xiao Yang, Roland Kwitt, and Marc Niethammer. Fast predictive image registration. In *Deep Learning and Data Labeling for Medical Applications*, pages 48–57. Springer, 2016.
- [76] Xiao Yang, Roland Kwitt, Martin Styner, and Marc Niethammer. Quicksilver: Fast predictive image registration—a deep learning approach. *NeuroImage*, 158:378–396, 2017.
- [77] Yongyue Zhang, Michael Brady, and Stephen Smith. Segmentation of brain mr images through a hidden markov random field model and the expectation-maximization algorithm. *IEEE transactions on medical imaging*, 20(1):45–57, 2001.
- [78] Amy Zhao, Guha Balakrishnan, Frédo Durand, John V. Guttag, and Adrian V. Dalca. Data augmentation using learned transforms for one-shot medical image segmentation. *CoRR*, abs/1902.09383, 2019.

Figure 12: Registration accuracy of anatomical structures for full-head T1 w-to-T1 w registration (HCP-A). Each box summarizes the label overlap for a specific structure across 30 test-image pairs of distinct subjects.

